Biochemical and Biophysical Research Communications 446 (2014) 1145–1150

Contents lists available at ScienceDirect

Biochemical and Biophysical Research Communications

journal homepage: www.elsevier.com/locate/ybbrc

Crystal structures of *Pseudomonas putida* esterase reveal the functional role of residues 187 and 287 in substrate binding and chiral recognition

Shuai Dou [a,b], Xu-Dong Kong [a,b], Bao-Di Ma [a], Qi Chen [a], Jie Zhang [a], Jiahai Zhou [b,c,*], Jian-He Xu [a,*]

[a] State Key Laboratory of Bioreactor Engineering, East China University of Science and Technology, Shanghai 200237, China
[b] Shanghai Institute of Organic Chemistry, Chinese Academy of Sciences, Shanghai 200032, China
[c] Key Laboratory of Combinatorial Biosynthesis and Drug Discovery, Wuhan University, Wuhan 430071, China

ARTICLE INFO

Article history:
Received 13 March 2014
Available online 27 March 2014

Keywords:
Crystal structure
Pseudomonas putida esterase
Enzyme-substrate complex
Chiral recognition
Activity enhancement
Protein engineering

ABSTRACT

A recombinant carboxylesterase (rPPE) from *Pseudomonas putida* ECU1011 was previously cloned and engineered to give a potential application for resolving chiral α-hydroxy acids including mandelic acids and derivatives. Two variants $rPPE_{W187H}$ and $rPPE_{D287A}$ showed a ~100-fold increase in activity towards *rac*-2-acetoxy-2-(2′-chlorophenyl) acetate (*rac*-AcO-CPA), but $rPPE_{D287A}$ had a significant decrease in enantioselectivity ($E = 8.7$) compared to $rPPE_{W187H}$ and the wild-type rPPE ($rPPE_{WT}$) ($E > 200$). Here we report the crystal structures of $rPPE_{WT}$ and $rPPE_{W187H}$, both by themselves and in complex with the substrate, to elucidate the structural basis of this phenomenon. An inactive mutation of nucleophile residue S159A was introduced to obtain the structure of $rPPE_{S159A/W187H}$ complexed with (*S*)-AcO-CPA. The structural analysis reveals that the side chain of residue Asp287 in $rPPE_{WT}$ would have a potential steric conflict with (*S*)-AcO-CPA when the substrate binds at the active site of the enzyme. However, the mutation W187H could facilitate the relocation of Asp287, while D287A directly eliminates the hindrance of Asp287, both of which offer sufficient space for the binding and hydrolysis of substrate. Moreover, Asp287 generates one site of the "three-point attachment model" as a hydrogen-bond donor that determines the excellent enantioselectivity of rPPE in chiral recognition, and D287A would obviously destroy the hydrogen bond and result in the low enantioselectivity of $rPPE_{D287A}$.

1. Introduction

With the rapid progress in resolving protein structures by X-ray diffraction or NMR spectroscopy, the number of enzyme structures deposited in Protein Data Bank is increasing enormously (around 50,000 up to date). As a strategy of protein engineering, rational or semi-rational design based on the structural information is increasingly important for the engineering of enzymes with industrial application potential [1,2]. Nowadays, even if there is no available structural data of the target enzyme, molecular modeling has been used to predict its structure using a homologous enzyme structure (if any) as template, which is widely applied in enzymes with conserved 3-dimensional structures, like enzymes of α/β hydrolase fold [3–5]. However, under many circumstances, the results of semi-rational design based on the predicted model are not completely consistent with the expectation. Even in the cases that improved performance (e.g., higher activity, better selectivity or stability) is successfully achieved with variants, we cannot always give a reasonable answer to how the mutation works with the predicted model, therefore unable to guide further engineering of the protein. In order to understand the molecular mechanism of enzymatic catalysis or reveal the basis of positive mutations from directed evolution and semi-rational design, accurate structural information by X-ray crystallography or NMR are indispensable [6].

Carboxylesterases (EC 3.1.1.1), widely distributed in animals, plants and microorganisms, are members of the α/β hydrolase family. They catalyze the hydrolysis of esters with short chain aliphatic or aromatic groups [7,8]. At present, they are widely used in industrial processes due to their broad substrate specificity and high regio- and enantioselectivity. In addition, a lot of carboxylesterases have shown high activity and stability in organic solvents, which are valuable properties for application in organic synthesis [9–11]. Among them, rPPE is a novel, thermostable and

Abbreviations: rPPE, recombinant *Pseudomonas putida* esterase; AcO-CPA, 2-acetoxy-2-(2′-chlorophenyl) acetate; MPD, 2-methyl-2,4-pentanediol; PEG, polyethylene glycol.

* Corresponding authors. Address: State Key Laboratory of Bioreactor Engineering, East China University of Science and Technology, Shanghai 200237, China.
E-mail addresses: jiahai@sioc.ac.cn (J. Zhou), jianhexu@ecust.edu.cn (J.-H. Xu).

http://dx.doi.org/10.1016/j.bbrc.2014.03.072
0006-291X/

organic-solvent tolerant carboxylesterase with a half-life of 14 days at 50 °C, capable of catalyzing the bioresolution of racemic 2-acetoxy-2-(2′-chlorophenyl)acetate (*rac*-AcO-CPA) with excellent enantioselectivity ($E > 200$). However, the high K_M (146 mM) and low k_{cat} (8.9 s^{-1}) of rPPE result in its low catalytic efficiency, which limits its application in industrial processes [12]. In our previous work, rational design based on homologous modeling and molecular docking generated two variants $rPPE_{W187H}$ and $rPPE_{D287A}$ which have 100- and 81-fold improvements in the catalytic efficiency (k_{cat}/K_M), respectively. However, only $rPPE_{W187H}$ retained the excellent enantioselectivity ($E > 200$), while the enantioselectivity of variant $rPPE_{D287A}$ decreased dramatically to $E = 8.7$ [13]. These results suggests that the residues at sites 187 and 287 have significant influence on the catalytic efficiency and chiral recognition, but the homologous model that we used could not afford a clear understanding of this phenomenon.

In this work, we resolved the crystal structures of wild-type rPPE ($rPPE_{WT}$, PDB: 4OB8) and $rPPE_{W187H}$ (PDB: 4OB7), which belong to the mammalian hormone-sensitive lipase (HSL) subfamily with α/β-hydrolase fold. We also introduced an inactive mutation S159A into $rPPE_{W187H}$ to obtain the structure of $rPPE_{S159A/W187H}$ in complex with substrate (*S*)-AcO-CPA (PDB: 4OB6). Structural analysis reveals the molecular mechanism behind the dramatic changes in activity and enantioselectivity of rPPE variants in detail. Moreover, structural information of rPPE allows a better understanding of its substrate recognition mechanism which is important for rational design of more robust biocatalysts.

2. Materials and methods

2.1. Protein expression and purification

The genes encoding rPPE variants [12] were cloned into a pET-21a(+) expression vector. Transformed *Escherichia coli* BL21(DE3) were grown overnight at 37 °C to provide a starter culture for expression. One liter medium was inoculated with 1% (v/v) of overnight culture and grown at 37 °C. When OD_{600} reached 0.6–0.8, the cultivation temperature was lowered to 25 °C and IPTG was added to a final concentration of 0.2 mM to induce protein overexpression. After 18 h, the cells were harvested by centrifugation (6000*g*) at 20 °C, and the cell pellet was resuspended in 50 ml lysis buffer (20 mM Tris–HCl, 500 mM NaCl, 5 mM 2-mercaptoethanol, 10 mM imidazole, pH 8.0), disrupted by sonication and the cell lysate was centrifuged (30,000*g*) at 4 °C for 40 min. The resulting supernatant was loaded onto a Ni–NTA column (5 ml) equilibrated with lysis buffer, and the retained protein was eluted with an increasing gradient from 10 to 500 mM imidazole in elution buffer at a flow rate of 5 ml/min. Then gel filtration was performed by chromatography on a Superdex 75 column (GE Healthcare) and eluted with Tris–HCl buffer (25 mM, pH 7.5) containing 150 mM NaCl and 1 mM DTT. SDS–PAGE analysis of the eluted protein revealed over 95% purity of the target protein, which was concentrated to around 32 mg/ml, and aliquots were immediately frozen in liquid nitrogen and stored at −80 °C.

2.2. Protein crystallization

Crystals of $rPPE_{WT}$, $rPPE_{S159A/W187H}$ and $rPPE_{W187H}$ were obtained by the sitting drop vapor diffusion method at 18 °C. Initial crystallization conditions were screened using Crystal Screen I & II Kits, Index kit (Hampton Research, USA) and Morpheus (Molecular dimensions, USA). The condition A of 0.1 M Hepes/Mops-Na, pH 7.5, 12.5% (w/v) PEG1000, 12.5% (w/v) PEG3350, 12.5% (v/v) MPD (2-methyl-2,4-pentanediol), 0.03 M $MgCl_2$, and 0.03 M $CaCl_2$ yielded the diffraction quality crystals after 2 days. The enzyme-substrate complex crystals of $rPPE_{S159A}$ and $rPPE_{S159A/W187H}$ were obtained under condition B consisting of 16% (w/v) PEG8000, 0.04 M KH_2PO_4, and 20% glycerol. Prior to cocrystallization, the proteins of $rPPE_{S159A}$ and $rPPE_{S159A/W187H}$ (0.94 mM or 32 mg/ml) were incubated with 100 mM sodium salt of (*S*)-AcO-CPA at 0 °C for 30 min. Before data collection, crystals were soaked in a cryoprotectant solution consisting of the reservoir solution and 10% (v/v) glycerol and then quickly frozen with liquid nitrogen.

2.3. Data collection and structure refinement

X-ray diffraction data were collected with flashly frozen crystals (at 100 K in a stream of nitrogen gas) on a RaxisIV++ imaging plate (Rigaku, TX, USA) using an in-house Rigaku MicroMax-007 HF rotating-anode X-ray generator operating at 40 kV and 30 mA. Diffraction data for the crystals were collected at 1.65–2.40 Å resolution, as shown in Table 1. The intensity sets were indexed, integrated and scaled with the HKL2000 package [14].

The $rPPE_{WT}$ structure was solved by molecular replacement method using Phaser [15] in the CCP4 crystallographic suite [16] with the crystal structure of esterase VA1 (PDB: 2YH2) as template. Several cycles of refinement were carried out using Phenix and Coot [17,18], progress in the structural refinement was evaluated by the free *R*-factor. The structures of $rPPE_{W187H}$, $rPPE_{S159A/W187H}$, $rPPE_{S159A}$-(*S*)-AcO-CPA complex, and $rPPE_{S159A/W187H}$-(*S*)-AcO-CPA complex were solved by molecular replacement using Phaser with the structure of $rPPE_{WT}$ as the search model.

2.4. Mutagenesis

Site-directed mutations of rPPE were constructed by Quick Change® Site-Directed Mutagenesis Kit, the mutagenic PCR was applied to the pET-21a(+) vector containing the gene of the $rPPE_{WT}$ and $rPPE_{W187H}$. For the mutation of M213A, the primers used were: 5′-ACCACCGGGATGGCGAAGTGG TTCTG-3′ (forward) and 5′-CAGAACCACTTCGCCATCCCGGTGGT-3′ (reverse). For the mutation of S159A, the primers used were: 5′-TGGCCGGCAACGCCGTTGGCGGCAACA-3′ (forward) and 5′-TGTTGCCGCCAACGGCGTTGCCGGCCA-3′ (reverse). The PCR products were transformed into *E. coli* DH5α and cultivated on the LB agar plate containing 100 mg/ml ampicillin. And the verified plasmid was transformed into *E. coli* BL21(DE3) for over-expression.

2.5. Activity assay using p-nitrophenyl esters

The activities of purified $rPPE_{WT}$ and $rPPE_{M213A}$ towards various *p*-nitrophenyl esters was assayed spectrophotometrically by measuring the initial rate of *p*-nitrophenol formation in enzymatic hydrolysis of 1 mM *p*-nitrophenyl ester in 100 mM sodium phosphate buffer (pH 7.0) at 30 °C [12]. One unit of activity was defined as the amount of enzyme that catalyzes the hydrolysis of 1.0 μmol *p*-nitrophenyl ester per minute under the assay condition.

3. Results

3.1. Overall structure of rPPE

The 1.8 Å resolution crystal structure of $rPPE_{WT}$ was determined in space group $P4_32_12$ with one molecule per asymmetric unit by molecular replacement method. Refinement of the structure finally converged with an *R*-factor of 0.1489 and *R*-free of 0.1823. The final model is comprised of 319 amino acids, one MPD (2-methyl-2,4-pentanediol) molecule, one PEG molecule and 365 water molecules. The rPPE molecule has an ellipsoidal shape with approximate dimensions of 51.3 Å × 42.5 Å × 38.4 Å (Fig. 1A). The

Table 1
Data collection and refinement statistics.

	rPPE	$rPPE_{W187H}$	$rPPE_{S159A/W187H}$	$rPPE_{S159A}$-(*S*)-AcO-CPA	$rPPE_{S159A/W187H}$-(*S*)-AcO-CPA
Data collection statistics					
Wavelength (Å)	1.5418	1.5418	1.5418	1.5418	1.5418
Space group	P43212	P43212	P43212	P43212	P43212
a (Å)	95.6	95.4	95.8	94.6	95.4
b (Å)	95.6	95.4	95.8	94.6	95.4
c (Å)	87.8	88.3	88.9	88.5	88.3
Resolution range (Å)[a]	42.8–1.80 (1.86–1.80)	42.0–1.65 (1.71–1.65)	38.6–1.99 (2.06–1.99)	42.3–2.40 (2.49–2.40)	33.7–1.70 (1.76–1.7)
Total/Unique reflections	38,145/3732	49,350/3205	28,983/1628	16,307/1896	45,435/2720
Redundancy[a]	25.5 (25.6)	15.4 (11.6)	17.8(17.2)	8.6 (8.7)	16.7 (16.2)
Average (I/δ)[a]	32.7 (9.6)	41.7 (5.1)	25.3 (3.6)	12.8 (3.0)	44.8 (8.4)
Completeness (%)[a]	99.6 (100)	99.5 (97.6)	99 (100)	100 (100)	100 (100)
R_{merge} (%)[b]	9.2 (41.0)	6.6 (49.6)	4.1 (12.2)	7.0 (80)	4.2 (41.2)
Refinement statistics					
PDB ID	4OB8	4OB7	4OU5	4OU4	4OB6
No. of reflections	38081	49281	28928	16258	45369
R-factor/*R*-free (%)[c]	14.9/18.2	15.6/17.3	14.2/17.6	16.8/23.3	16.4/18.1
Average B factor (Å²)					
Protein atoms	24	21	24	34	22
Solvent atoms	36	31	35	37	29
MPD	23.2	23.3	26.8	–	–
PEG	41.6	35.6	43.2	–	–
(S)-AcO-CPA	–	–	–	54.2	30.1/42.5/35.9
R.m.s deviations from ideal geometry					
Bond lengths (Å)	0.006	0.006	0.007	0.008	0.007
Bond angles (°)	1.074	1.060	1.035	1.126	1.191
Ramachandran plot					
Favored (%)	98.1	97.8	97.2	95.0	97.5
Allowed (%)	1.9	2.2	2.8	4.7	2.2
Disallowed (%)	0	0	0	0.3	0.3

[a] Numbers in parentheses are values for the highest-resolution shell.
[b] $R_{merge} = \sum_{hkl}|I_i - I_m|/I_{hkl}I_m$, where I_i and I_m are the observed intensity and the mean intensity of related reflections, respectively. Values in parentheses indicate high-resolution shell.
[c] *R*-factor = $\sum||F_o - F_c||/acF_o|$. $R_{free} = \sum_T||F_o - F_c||/e_T|F_o|$, where *T* is a test data set of 5% of the total reflections randomly chosen and set aside prior to refinement.

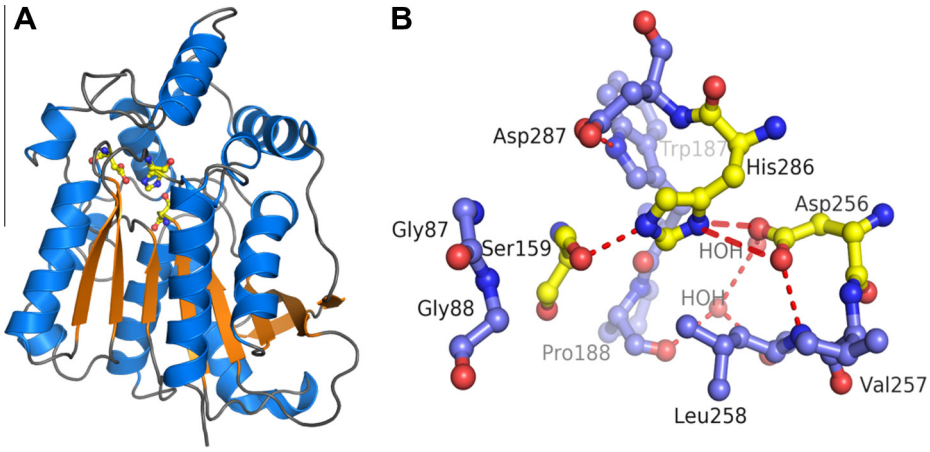

Fig. 1. The crystal structure of rPPE. (A) Overall structure of rPPE, the catalytic triad is colored in yellow. (B) Stereo diagram of the active center of rPPE. The catalytic triad is shown in yellow sticks. Hydrogen bond network around the catalytic triad is presented as red dashed line. (For interpretation of the references to color in this figure legend, the reader is referred to the web version of this article.)

crystallographic statistics for data collection and refinement are summarized in Table 1.

The structure of rPPE consists of a core domain, belonging to the α/β hydrolase fold family, and a cap domain, analogous to those present in the other members of the HSL family [19,20]. When compared with the generalized α/β-hydrolase fold described by Ollis et al., rPPE obeys the canonical α/β-hydrolase fold with central eight-stranded β-sheet surrounded by α-helices on both sides (only strand β2 is antiparallel) (Fig. 1A). The β1 and β8 strands are approximately perpendicular to each other because of the counter clockwise twist of the β-sheet. The cap domain is formed by the clustering of two *N*-terminal α-helices (α1 and α2) and two α-helices (α6 and α7) following strand β6, and located at the upper region of the central β-sheet (Fig. S1b).

3.2. Catalytic triad and substrate binding pocket

By sequence and structural alignment, the catalytic triad of rPPE was identified as Ser159, Asp256, and His286. Ser159 is in the conserved Gly-X-Ser-X-Gly motif [21], and is located at the nucleo-

philic elbow between strand β5 and helix α5. Its conformation is stabilized by the hydrogen bond between its OG atom and NE2 atom (atoms were named as in PDB file) of His286 at 2.7 Å distance (Fig. 1B). His286 is located in a five-residue loop, connecting strand β8 to helix α9. Its ND1 atom is hydrogen bonded to the OD1 and OD2 atom of Asp256 at 3.4 Å and 2.8 Å distance, respectively. Asp256 is the third member of the catalytic triad, and is located between strand β7 and helix α8 (Fig. S1b). The side chain of Asp256 is further stabilized by a hydrogen bond between its OD1 atom and the NH atom of Leu258 (2.9 Å), and a hydrogen bond between its OD2 atom and the water molecule HOH13 (2.7 Å), which in turn interacts with HOH5 (3 Å). HOH5 is hydrogen bonded to the carbonyl oxygen atoms of both Leu258 (2.9 Å) and Pro188 (2.73 Å). These water molecules are strictly conserved within the HSL family [19,22], forming the center of a hydrogen bonding networks which stabilize the active site pocket by connecting the *C*-terminal end of strand β7 and the *N*-terminal end of helix α8.

Based on the observation of the solvent accessible surface, a cavity could be identified between helix α1 and α2 of the cap domain, leading to the active center of rPPE (Fig. S2). The nucleophile residue (Ser159) of active site lies at the bottom of this hydrophobic cavity, which has a funnel shape with approximate dimension of 13 Å × 10 Å on top and 17 Å in depth. The residues from loop region (Gly86–Gly88, Phe207–Thr209, Ile285–Asp287) and helix α7 (Met212–Phe216) act as internal borders of this cavity. By comparing with structures of other HSL family members, rPPE has a significant hindrance in the acyl part of substrate binding pocket (Fig. S3). Accordingly, mutation M213A was introduced at the bottom of the funnel to extend the acyl binding pocket which would facilitate rPPE to catalyze the hydrolysis of esters with relatively larger acyl group. As shown in Fig. 2, the substrate preference of $rPPE_{M213A}$ towards *p*-nitrophenyl esters was shifted as expected. For substrate *p*NPB with a large four-carbon acyl group, a 63-fold higher activity was observed with $rPPE_{M213A}$, while its activity towards substrate *p*NPA with a small two-carbon acyl group decreased over 40-fold, when compared with the $rPPE_{WT}$. However, for the ester substrate with an even larger six-carbon acyl group, the activity of $rPPE_{M213A}$ (0.063 U/mg) became negligible, but also has a 30-fold improvement compared with $rPPE_{WT}$ (0.002 U/mg), impling that the space of acyl binding pocket is still limited for esters with larger acyl group, probably by hindrance of residues such as Val160 and Trp89.

3.3. Crystal structure of $rPPE_{W187H}$

The variant $rPPE_{W187H}$ was crystallized readily under the same condition as that for $rPPE_{WT}$, and its structure was determined at a resolution of 1.65 Å. Just like in $rPPE_{WT}$, one MPD molecule could be found in the funnel shape cavity leading to the active site, with a distance of 5.7 Å to the nucleophile residue Ser159. The three-dimensional structure of $rPPE_{W187H}$ is very similar to that of $rPPE_{WT}$ (Rmsd = 0.062 Å) except the side chain of the mutated residue, the residues of the catalytic triad or those around the mutation site have no conformational change (Fig. 3A).

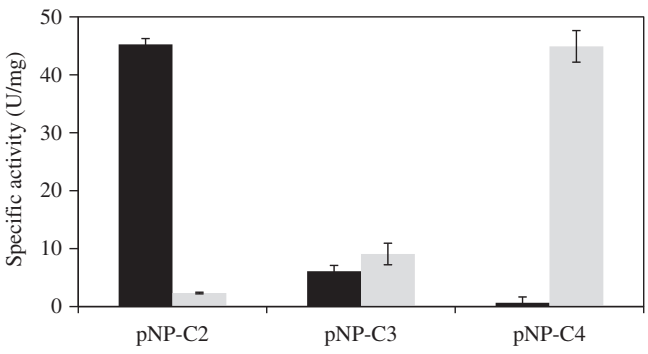

Fig. 2. Substrate preference of rPPE and $rPPE_{M213A}$ for *p*-nitrophenyl esters. The activity of purified enzymes towards various *p*-nitrophenyl esters were determined spectrophotometrically. ■, $rPPE_{WT}$; ■, $rPPE_{M213A}$.

3.4. Complex structure of $rPPE_{S159A/W187H}$ with (*S*)-AcO-CPA

To obtain enzyme-substrate complex structure, we introduced an inactive mutation of nucleophile S159A in $rPPE_{WT}$ and $rPPE_{W187H}$. The structure of $rPPE_{S159A/W187H}$ complexed with substrate was solved by molecular replacement using the coordinates of $rPPE_{WT}$ as the searching model. The final structure was refined to a crystallographic *R*-factor of 0.164 and an *R*-free of 0.181 in the resolution of 33.7–1.70 Å resolution range. Three (*S*)-AcO-CPA molecules were identified, with the first one binded at the active center (Fig. 3B), the second one located at the entrance of the binding pocket and the third one being on the surface of the protein. By structural alignment, we found that the side chain of Asp287 in the complex structure has a significant motion of 2.2 Å, and it interacts closely with the ionized carboxyl group of the substrate (Fig. 3C). Meanwhile the side chain of His187 moves significantly (2.3 Å) in the same direction to offer enough space for Asp287. To confirm the alteration is resulted from the binding of substrate, rather than the mutation of S159A, we further determined the structure of $rPPE_{S159A/W187H}$ containing no substrate. In the native structure of $rPPE_{S159A/W187H}$, no significant conformational change could be found, as has been observed in the complex structure. Moreover, we solved the structure of $rPPE_{S159A}$ co-crystallized with substrate, and found an unmodeled density in the acyl binding region and one (*S*)-AcO-CPA molecule on the surface of the protein (Fig. S4). The unmodeled density suggests a very low occupancy of the substrate molecule, which is coincident with the low binding affinity of $rPPE_{WT}$ with (*S*)-AcO-CPA [13]. As expected, no conformational change was observed around both sites Asp287 and Trp187.

4. Discussion

4.1. Origins of activity enhancement in $rPPE_{W187H}$ and $rPPE_{D287A}$

What causes the striking difference in catalytic performance between the $rPPE_{WT}$ and variants rPPEW187H and rPPED287A, when only a single mutation was introduced? Based on the detail structural information reported here, one straightforward explanation might be the reduced steric hindrance facilitates the access of substrate to the active site in rPPE. By superimposing the native structures of $rPPE_{WT}$ and rPPEW187H with the complex structure $rPPE_{S159A/W187H}$-(*S*)-AcO-CPA, respectively, we found that the ionized carboxyl group of substrate would have a potential steric conflict with the side chain of residue Asp287. In variant $rPPE_{W187H}$, this conflict is removed by the relocation of side chain of Asp287 and His187. However, there was no sufficient space for the indole ring of Trp187 to move flexibly in $rPPE_{WT}$ (Fig. 3D), which prevents the relocation of the side chain of Asp287 and consequently hinders the effective binding of substrate in the active center. Therefore, a 7.3-fold decrease in KM combined with a 13.8-fold increase in k_{cat} contributed to a total 100-fold increase in $k_{cat/KM}$ of rPPEW187H [13]. For variant rPPED287A, since the steric hindrance is significantly reduced by the single mutation D287A, its substrate binding affinity has a 34-fold increase compared with $rPPE_{WT}$ [13].

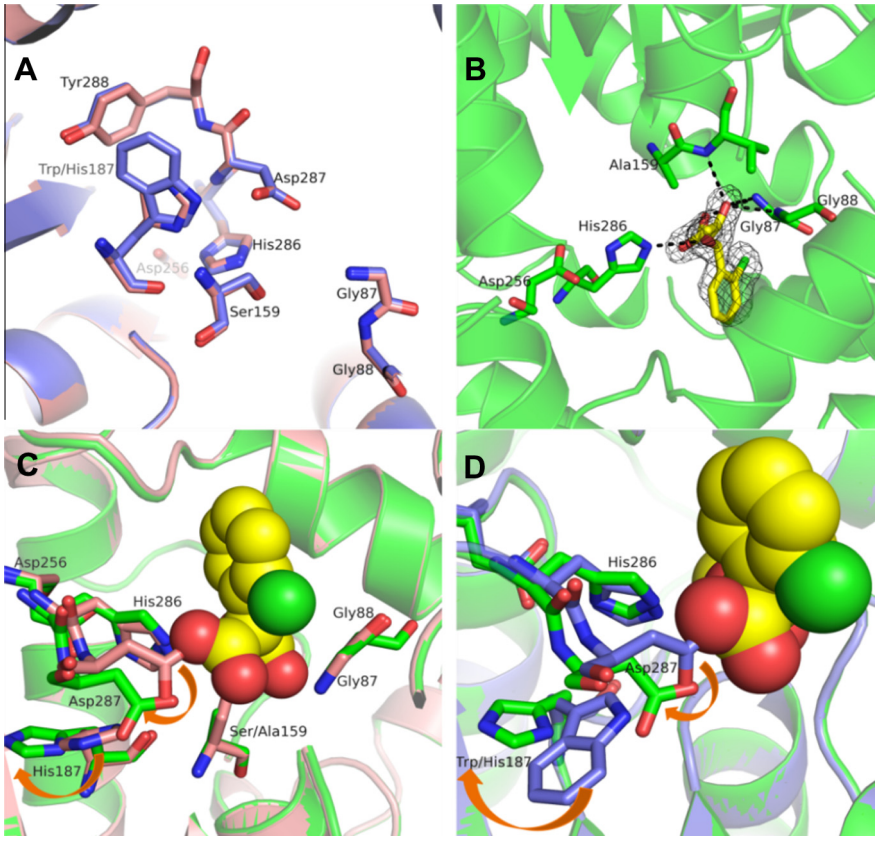

Fig. 3. Crystal structure of the $rPPE_{S159A/W187H}$-substrate complex. (A) Structural comparison of active site residues between $rPPE_{W187H}$ (deep salmon) and $rPPE_{WT}$ (bule). (B) Details of the interaction of $rPPE_{S159A/W187H}$ with (*S*)-AcO-CPA in the active site. The $F_o - F_c$ electron density map of ligand contoured at 1.0σ is shown in black mesh. (C) Superposition of $rPPE_{S159A/W187H}$-(*S*)-AcO-CPA (green) and $rPPE_{W187H}$ (deep salmon). The red arrows represent the relocation of side chain of His187 and Asp287 caused by the substrate binding. (D) Superposition of $rPPE_{S159A/W187H}$-(*S*)-AcO-CPA (green) and $rPPE_{WT}$ (bule). The red arrows represents the different conformation of side chain of residue 187 and Asp287 in $rPPE_{WT}$ and in $rPPE_{S159A/W187H}$-(*S*)-AcO-CPA complex. (For interpretation of the references to color in this figure legend, the reader is referred to the web version of this article.)

4.2. Chiral recognition of rPPE

In our previous work, mutation D287A significantly increased the substrate binding affinity of rPPE by 34-folds, but the *E* value was significantly decreased (from >200 to 8.7) [13]. Based on the complex structure, we supposed that Asp287 not only plays a vital role in the substrate binding, but also is very important for guaranteeing the excellent enantioselectivity of rPPE. The distance between the ionized carboxyl group of substrate and the side chain of Asp287 is 2.6 Å. As calculated by PROPKA, in the complex structure of $rPPE_{S159A/W187H}$-(*S*)-AcO-CPA, the pK_a values of Asp287 and substrate are 9.9 and 3.8, respectively. The pK_a values suggests that when the substrate binds to the enzyme , Asp287 should be in the protonized state while the ionized carboxyl group of substrate should be deprotonized, and there should be a strong hydrogen bond between them. Under this assumption, the "three-point attachment theory" put forward by A.G. Ogston (1948) can provide us a better understanding of the mechanism of rPPE for chiral recognition and high enantioselectivity. During the substrate binding process, three substituent groups of the chiral carbon atom in substrate are spatially fixed by the active site of rPPE, which determines the preference of rPPE for (*S*)-configuration substrate (Fig. 4). Firstly, the carbonyl group of ester bond is stabilized by oxyanion hole with three hydrogen bonds. Secondly, the ionized (or deprotonized) carboxyl group of substrate forms a hydrogen bond with Asp287. Lastly, the space left in the active site for accommodating the H atom of chiral carbon atom is very limited, therefore sterically preventing the mis-location of any large group

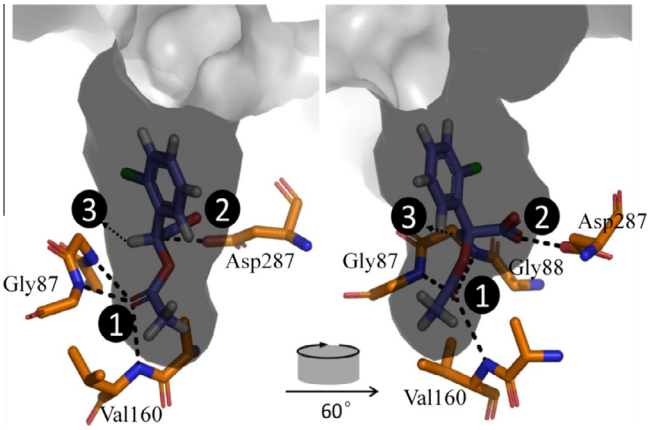

Fig. 4. Three-point-attachment model of chiral recognition. The substrate (*S*)-AcO-CPA is shown in blue; the residues participated in chiral recognition is shown in orange. Point one: the oxygen atoms of the carboxyl groups is stabilized by oxyanion hole; point two: the ionized carboxyl group of substrate has a hydrogen bond with Asp287; point three: the space left in the active site for accommodating the H atom is very limited. (For interpretation of the references to color in this figure legend, the reader is referred to the web version of this article.)

on this position and making the bulky *othro*-chlorophenyl group located compulsively in the external and wider side of the substrate access cavity. Based on this assumption, the active site of rPPE allows the substituent groups of (*S*)-substrate to bind well into a definite spatial arrangement of the active site and excludes

the possibility of (*R*)-enantiomer's mis-binding, naturally resulting an excellent enantioselectivity. When the residue Asp287 was replaced by alanine in variant $rPPE_{D287A}$, the active site of the enzyme would lose one effective point of attachment, the expanded space around residue 287 might allow *othro*-chlorophenyl group to access this position. Therefore, there will be only "two-point attachment" between the enzyme and the substrate, which would necessarily lead to a severe decrease in the enantioselectivity of $rPPE_{D287A}$.

In conclusion, our work not only explains the reason for activity changes of variants $rPPE_{W187H}$ and $rPPE_{D287A}$ but also reveals the mechanism for chiral recognition of rPPE. The results reported here are interesting from either a theoretical or biotechnological point of view, and provide vital structural information for further engineering of this enzyme as well as other closely related α/β hydrolases to improve their catalytic efficiency and/or enantioselectivity.

Acknowledgments

This work was financially supported by the National Natural Science Foundation of China (No. 21276082), Ministry of Science and Technology, P.R. China (Nos. 2011CB710800, 2011AA02A210 and 2012AA022201), and Shanghai Commission of Science and Technology (No. 11431921600). We thank Gong Y. for the excellent work in maintaining the in-house X-ray machine.

Appendix A. Supplementary data

Supplementary data associated with this article can be found, in the online version, at http://dx.doi.org/10.1016/j.bbrc.2014.03.072.

References

[1] L.G. Otten, F. Hollmann, I.W.C.E. Arends, Enzyme engineering for enantioselectivity: from trial-and-error to rational design, Trends Biotechnol. 28 (2010) 46–54.
[2] R.A. Chica, N. Doucet, J.N. Pelletier, Semi-rational approaches to engineering enzyme activity: combining the benefits of directed evolution and rational design, Curr. Opin. Biotechnol. 16 (2005) 378–384.
[3] R.J. Kazlauskas, U.T. Bornscheuer, Finding better protein engineering strategies, Nat. Chem. Biol. 5 (2009) 526–529.
[4] S. Lutz, Beyond directed evolution—semi-rational protein engineering and design, Curr. Opin. Biotechnol. 21 (2010) 734–743.
[5] H. Jochens, M. Hesseler, K. Stiba, S.K. Padhi, R.J. Kazlauskas, U.T. Bornscheuer, Protein engineering of α/β-hydrolase fold enzymes, ChemBioChem 12 (2011) 1508–1517.
[6] M. Ferraroni, I. Matera, S. Burger, S. Reichert, L. Steimer, A. Scozzafava, A. Stolz, F. Briganti, The salicylate 1,2-dioxygenase as a model for a conventional gentisate 1,2-dioxygenase: crystal structures of the G106A mutant and its adducts with gentisate and salicylate, FEBS J. 280 (2013) 1643–1652.
[7] D.M. Charbonneau, F. Meddeb-Mouelhi, M. Beauregard, A novel thermostable carboxylesterase from *Geobacillus thermodenitrificans*: evidence for a new carboxylesterase family, J. Biochem. 148 (2010) 299–308.
[8] P. Liu, H.E. Ewis, P.C. Tai, C.-D. Lu, I.T. Weber, Crystal structure of the *geobacillus stearothermophilus* carboxylesterase Est55 and its activation of prodrug CPT-11, J. Mol. Biol. 367 (2007) 212–223.
[9] M.T. Reetz, Lipases as practical biocatalysts, Curr. Opin. Chem. Biol. 6 (2002) 145–150.
[10] U.T. Bornscheuer, Microbial carboxyl esterases: classification, properties and application in biocatalysis, FEMS Microbiol. Rev. 26 (2002) 73–81.
[11] S. Cherif, Y. Gargouri, An organic-solvent-tolerant esterase from turkey pharyngeal tissue, Bioresour. Technol. 101 (2010) 3732–3736.
[12] B.D. Ma, H.L. Yu, J. Pan, J.Y. Liu, X. Ju, J.H. Xu, A thermostable and organic-solvent tolerant esterase from *Pseudomonas putida* ECU1011: catalytic properties and performance in kinetic resolution of alpha-hydroxy acids, Bioresour. Technol. 133 (2013) 354–360.
[13] B.D. Ma, X.D. Kong, H.L. Yu, Z.J. Zhang, S. Dou, Y.P. Xu, Y. Ni, J.H. Xu, Increased catalyst productivity in α-hydroxy acids resolution by esterase mutation and substrate modification, ACS Catal. 4 (2014) 1026–1031.
[14] Z. Otwinowski, W. Minor, Processing of X-ray diffraction data collected in oscillation mode, in: Charles W. Carter Jr. (Ed.), Methods in Enzymology, Academic Press, 1997, pp. 307–326.
[15] A.J. McCoy, R.W. Grosse-Kunstleve, P.D. Adams, M.D. Winn, L.C. Storoni, R.J. Read, Phaser crystallographic software, J. Appl. Crystallogr. 40 (2007) 658–674.
[16] L. Potterton, S. McNicholas, E. Krissinel, J. Gruber, K. Cowtan, P. Emsley, G.N. Murshudov, S. Cohen, A. Perrakis, M. Noble, Developments in the CCP4 molecular-graphics project, Acta Crystallogr. D 60 (2004) 2288–2294.
[17] G.N. Murshudov, A.A. Vagin, E.J. Dodson, Refinement of macromolecular structures by the maximum-likelihood method, Acta Crystallogr. D 53 (1997) 240–255.
[18] P. Emsley, K. Cowtan, Coot: model-building tools for molecular graphics, Acta Crystallogr. D 60 (2004) 2126–2132.
[19] G. De Simone, S. Galdiero, G. Manco, D. Lang, M. Rossi, C. Pedone, A snapshot of a transition state analogue of a novel thermophilic esterase belonging to the subfamily of mammalian hormone-sensitive lipase, J. Mol. Biol. 303 (2000) 761–771.
[20] Y. Wei, J.A. Contreras, P. Sheffield, T. Osterlund, U. Derewenda, R.E. Kneusel, U. Matern, C. Holm, Z.S. Derewenda, Crystal structure of brefeldin A esterase, a bacterial homolog of the mammalian hormone-sensitive lipase, Nat. Struct. Mol. Biol. 6 (1999) 340–345.
[21] H. Hemilä, T.T. Koivula, I. Palva, Hormone-sensitive lipase is closely related to several bacterial proteins, and distantly related to acetylcholinesterase and lipoprotein lipase: identification of a superfamily of esterases and lipases, Biochim. Biophys. Acta, Lipids Lipid Metab. 1210 (1994) 249–253.
[22] G. De Simone, V. Menchise, G. Manco, L. Mandrich, N. Sorrentino, D. Lang, M. Rossi, C. Pedone, The crystal structure of a hyper-thermophilic carboxylesterase from the archaeon *Archaeoglobus fulgidus*, J. Mol. Biol. 314 (2001) 507–518.